ASN NEURO RESEARCH ARTICLE

Supplementary data

ASN NEURO 3(5):art:e00071.doi:10.1042/AN20110025

# Early astrocytic atrophy in the entorhinal cortex of a triple transgenic animal model of Alzheimer's disease

**Chia-Yu Yeh*, Bhamini Vadhwana†, Alexei Verkhratsky*,‡,§,‖,¶ and José J Rodríguez‡,§,‖,¶1**

*Faculty of Life Sciences, The University of Manchester, Manchester, U.K.
†The School of Medicine, The University of Manchester, Manchester, U.K.
‡IKERBASQUE, Basque Foundation for Science, 48011 Bilbao, Spain
§Instituto de Investigación Sanitaria Biodonostia, Hospital Donostia and Centro de Investigaciones Biomédicas en Red Enfermedades Neurodegenerativas (CIBERNED), 20014 San Sebastián, Spain
‖Department of Neurosciences, University of the Basque Country UPV/EHU, 48940 Leioa, Spain
¶Institute of Experimental Medicine, ASCR, Videnska 1083, 142 20 Prague, Czech Republic

**Cite this article as:** Yeh C-Y, Vadhwana B, Verkhratsky A and Rodríguez JJ (2011) Early astrocytic atrophy in the entorhinal cortex of a triple transgenic animal model of Alzheimer's disease. ASN NEURO 3(5):art:e00071.doi:10.1042/AN20110025

## ABSTRACT

The EC (entorhinal cortex) is fundamental for cognitive and mnesic functions. Thus damage to this area appears as a key element in the progression of AD (Alzheimer's disease), resulting in memory deficits arising from neuronal and synaptic alterations as well as glial malfunction. In this paper, we have performed an in-depth analysis of astroglial morphology in the EC by measuring the surface and volume of the GFAP (glial fibrillary acidic protein) profiles in a triple transgenic mouse model of AD [3xTg-AD (triple transgenic mice of AD)]. We found significant reduction in both the surface and volume of GFAP-labelled profiles in 3xTg-AD animals from very early ages (1 month) when compared with non-Tg (non-transgenic) controls (48 and 54%, reduction respectively), which was sustained for up to 12 months (33 and 45% reduction respectively). The appearance of A$\beta$ (amyloid $\beta$-peptide) depositions at 12 months of age did not trigger astroglial hypertrophy; nor did it result in the close association of astrocytes with senile plaques. Our results suggest that the AD progressive cognitive deterioration can be associated with an early reduction of astrocytic arborization and shrinkage of the astroglial domain, which may affect synaptic connectivity within the EC and between the EC and other brain regions. In addition, the EC seems to be particularly vulnerable to AD pathology because of the absence of evident astrogliosis in response to A$\beta$ accumulation. Thus we can consider that targeting astroglial atrophy may represent a therapeutic strategy which might slow down the progression of AD.

Key words: Alzheimer's disease, astrocyte, dementia, entorhinal cortex, glial fibrillary acidic protein (GFAP), memory.

## INTRODUCTION

The EC (entorhinal cortex), a part of the temporal cortex, is involved in mnesic processes by establishing the cortico-hippocampal circuits. The EC is divided into superficial (I–III) and deep layers (IV–VI) that show differential anatomical and functional organization (Suzuki and Amaral, 1994; Witter and Amaral, 2004). The superficial layers are the main recipient of intracortical information and the major output source to the HC (hippocampus), whereas the deep layers are mainly responsible for the projections to cortical regions (Figure 1; Suzuki and Amaral, 1994; Witter and Amaral, 2004). The neurons from the EC layer II terminate in the middle and outer molecular layer of the DG (dentate gyrus) and send collaterals to the hippocampal CA2 and CA3 fields (Witter et al., 1989; Tamamaki and Nojyo, 1993; Suzuki and Amaral, 1994). Layer III neurons project mainly to the CA1 and subiculum, which in turn feedback to layer V of the EC (Naber et al., 2001). Functionally, activation of the EC and persistent neuronal activity in the EC are involved in the

[1] To whom correspondence should be addressed (email j.rodriguez-arellano@ikerbasque.org).

**Abbreviations:** AD, Alzheimer's disease; A$\beta$, amyloid $\beta$-peptide; EC, entorhinal cortex; GFAP, glial fibrillary acidic protein; GFAP-IR, glial fibrillary acidic protein-immunoreactive; HC, hippocampus; LEC, lateral entorhinal cortex; NFT, neurofibril tangle; non-Tg, non-transgenic; Nv, numerical density; PB, phosphate buffer; PHF, paired helical filament; RT, room temperature; SP, senile plaque; 3xTg-AD, triple transgenic mice of AD; TS, Tizma-based saline.

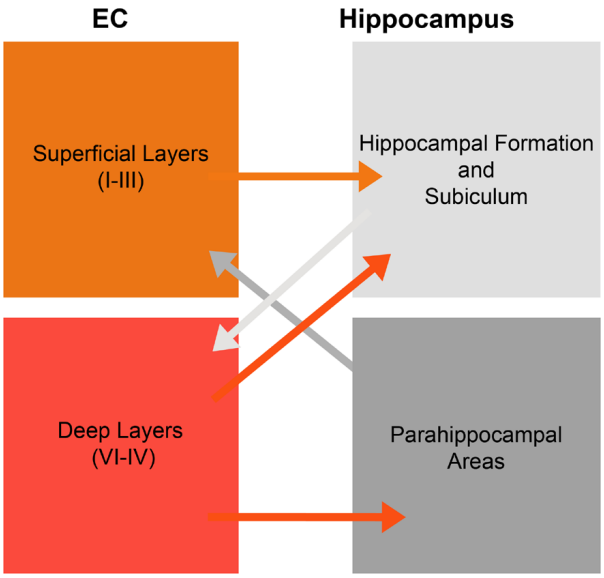


**Figure 1 Schematic illustration of entorhinal inputs to the HC**
In brief, the superficial layers (I–III) project to the hippocampal formation and subiculum, while the deep layers (V/VI) receive reciprocal inputs from these areas. Meanwhile, deep layers also innervate to parahippocampal areas and the HC.

process of working memory (Ranganath et al., 2003; Fransen, 2005; McGaughy et al., 2005). The EC is also essential for memory consolidation (Remondes and Schuman, 2004; Craig and Commins, 2005) and spatial navigation and memory (Fyhn et al., 2004; Moser et al., 2008).

Entorhinal dysfunction is involved in several brain diseases that compromise cognitive and memory functions, including AD (Alzheimer's disease) (Braak and Braak, 1991; Kril et al., 2002; Schwarcz and Witter, 2002; Cunningham et al., 2006). The AD is an irreversible neurodegenerative disease accompanied by cognitive/memory impairments, which is the most common cause of progressive dementia in elderly people (Braak and Braak, 1991; Braak et al., 1999; Harciarek and Jodzio, 2005). AD is characterized by the appearance of SPs (senile plaques) representing extracellular A$\beta$ (amyloid $\beta$-peptide) depositions (Nagele et al., 2004) and NFTs (neurofibril tangles) consisting of abnormally hyperphosphorylated tau protein, the latter being a major microtubule-associated protein (Schneider and Mandelkow, 2008). The EC is affected very early by AD pathology; it is arguably the first brain region experiencing A$\beta$ accumulation (Braak and Braak, 1991, 1997; Thal et al., 2000). Similarly, the NFTs appear in the transentorhinal region and in the EC at the early stages of AD (Braak stages I/II) and are widespread in the EC at middle Braak stages (limbic stages III/IV) (Solodkin et al., 1996; Braak and Braak, 1997). Concomitant with the presence of A$\beta$ and NFTs in the EC, this cortical region undergoes severe volume decrease that also affects its major projection target, the HC (Du et al., 2001; Halliday et al., 2003; Whitwell et al., 2008). Profound neuronal loss, mainly in layer II, also occurs in AD concomitantly with mild cognitive impairment (Gomez-Isla et al., 1996; de Toledo-Morrell et al., 2000; Du et al., 2001; Rodrigue and Raz, 2004).

The AD-related neuronal loss and atrophy of the EC are well documented in human patients (Gomez-Isla et al., 1996; Calhoun et al., 1998; de Toledo-Morrell et al., 2000; Du et al., 2001; Kordower et al., 2001; Ribe et al., 2005). However, little is known about AD-associated changes in EC astroglia. Post-mortem studies have revealed an increase in GFAP (glial fibrillary acidic protein) protein levels as well as in the number of GFAP-positive astrocytes within the EC, which seems to be associated with the A$\beta$ load (Muramori et al., 1998; Porchet et al., 2003). Recently, we reported the concomitant occurrence of astroglial atrophy and astrogliosis in the HC of the transgenic mice model of AD. The atrophy appears as a generalized process, whereas astrogliosis was triggered by developing SPs and A$\beta$ aggregates (Rodríguez et al., 2009b; Heneka et al., 2010; Olabarria et al., 2010; Verkhratsky et al., 2010; Rodríguez and Verkhratsky, 2011). In the present paper, we extended our analysis of AD-associated changes in astroglia to the EC.

## MATERIALS AND METHODS

All animal procedures were carried out in accordance with the United Kingdom Animals (Scientific Procedures) Act of 1986 under license from the Home Office. All efforts were made to reduce the number of animals by following the 3R's.

### Animal models

The generation of 3xTg-AD (triple transgenic mice of AD) mice has been well described (Oddo et al., 2003a, 2003b; Billings et al., 2005; Rodríguez et al., 2008; Rodríguez et al., 2009a, 2009b). The 3xTg-AD mice were derived from mixed 129/C57BL6 mice, which harbour APPswe, PS1M146V and TauP301L mutations, and the same spatiotemporal progression of amyloid and tau protein pathology in human AD. The non-Tg (non-transgenic) control mice were from the same strain and the same genetic background. All 3xTg-AD and non-Tg littermates were from homozygous breeders. Mice were grouped by gender and genotype, housed under controlled temperature and 12 h light/12 h dark cycles with *ad libitum* access to food and water.

### Fixation and tissue processing

As previously described (Olabarria et al., 2010), male 3xTg-AD at 1, 3, 6, 9 and 12 months of age ($n$=5, 4, 4, 5 and 5 respectively) and their age-corresponding non-Tg controls ($n$=4, 4, 4, 5, 5 respectively) were anaesthetized with sodium pentobarbital (50 mg/kg) intraperitoneally. The brains were fixed by aortic arch perfusion of 3.75% acrolein (25 ml; TAAB, UK) in 2% (w/v) paraformaldehyde (Sigma, St. Louis, MO, U.S.A.) and 0.1 M PB (phosphate buffer) at pH 7.4, followed by 75 ml of 2% paraformaldehyde. Brains were removed, cut into 2–3 mm

coronal slabs containing the EC, post-fixed in 2% paraformaldehyde for 24 h and sectioned at 40–50 μm with a vibrating microtome (VT1000S; Leica, Milton Keynes, U.K.). Free-floating sections in 0.1 M PB were collected and stored in a cryoprotectant solution containing 25% sucrose and 3.5% glycerol in 0.05 M PB at pH 7.4. Coronal sections at levels −2.30 mm/−3.88 mm [LEC (lateral entorhinal cortex)] posterior to Bregma were selected for immunohistochemistry according to the mouse brain atlas of Paxinos and Franklin (2004).

## Antibodies

To detect and determine the changes in the astrocytic cytoskeleton in the EC, we used a monoclonal mouse antiserum against GFAP (anti-GFAP; Sigma–Aldrich; #G3893). For the identification of A$\beta$ aggregation as well as the relation of astrocytic cytoskeleton alteration with A$\beta$, we used a polyclonal rabbit anti-GFAP serum (Sigma–Aldrich; #G9269) and a monoclonal mouse antiserum against amino acid residues 1–16 of A$\beta$, which reacts with abnormally processed isoforms and precursor form of A$\beta$ [EFRHDS; anti-A$\beta$ 6E10 (SIG-39320), Signet Laboratories, Dedham, MA, U.S.A.]. For the detection of NFTs, we used a monoclonal mouse antiserum against PHF (paired helical filament) tau protein, which recognizes phosphorylated Ser-202/Thr-205 of tau protein (Innogenetics, Zwijndrecht, Belgium). The immunolabelling pattern we obtained with this antibody is equivalent to that obtained previously in different brain regions (Oddo et al., 2003a). Positive and negative control immunohistochemistry was used to test non-specific labelling and/or cross-reaction between antisera derived from different host species, showing no immunoreactivity (data not shown). The specificity of these antisera was confirmed by immunohistochemistry and Western blotting in previous papers (Goedert 1995; Halliday et al., 1996; Rodríguez et al, 2008).

## Immunocytochemistry

The procedure for immunocytochemistry was as described previously (Olabarria et al., 2010; Noristani et al., 2010). All sections from both non-Tg and 3xTg-AD groups at different ages were processed at the same time using precisely the same experimental conditions to minimize methodological variability. Sections were pretreated with 30% (v/v) methanol and 3% $H_2O_2$ in 0.1 M PB for 30 min and subsequently a 1% sodium borohydride (Sigma–Aldrich) solution for 30 min. After washing with PB profusely, sections were then rinsed with 0.1 M TS (Tizma-based saline; Sigma–Aldrich), followed by incubation in 0.5% BSA (Sigma–Aldrich) and 0.25% Triton X-100 (Sigma) for 30 min. The sections were incubated in 0.1% BSA in 0.1 M TS at pH 7.6 and 0.25% Triton X-100 containing the following antibodies: monoclonal mouse anti-GFAP (1:5000; Sigma), monoclonal mouse anti-A$\beta$ (1:1000; Covance, Emeryville, CA, U.S.A.) or monoclonal mouse anti-PHF tau protein (1:1000; Innogenetics) at room temperature (RT) (20–25 °C) for 48 h. The sections were rinsed with TS and incubated in biotinylated horse anti-mouse IgG (1:200; Vector Laboratories, Peterborough, U.K.) at RT for 1 h. After rinsing with TS for 30 min, sections were incubated with avidin–biotin peroxidase complex (Vector Laboratories). The peroxidase reaction was carried out by incubation with a solution containing 0.022% DAB (diaminobenzidine; Aldrich) or 0.003% $H_2O_2$, or the SG peroxidase substrate kit (Vector Laboratories) for 5 min. Sections were then dehydrated in ascending concentration of ethanol (50, 70, 80, 90, 95 and 100%) and subsequently xylene, and then permanently coverslipped with the use of Entellan (Merck).

For single fluorescent labelling, the sections were then incubated for 48 h at RT in the primary antibody solution as mentioned above. Sections were then rinsed with 0.1 M TS and incubated in secondary solution containing FITC-conjugated goat anti-mouse IgG (1:100; Jackson Immunoresearch, Baltimore Pike, PA, U.S.A.) for 1 h at RT.

For dual labelling, the sections were incubated for 48 h at RT in a primary antibody cocktail containing (i) monoclonal mouse anti-A$\beta$ antibody (1:1000; Covance) and (ii) rabbit anti-GFAP (1:5000; Sigma) simultaneously. Sections were washed with 0.1 M TS and incubated in rhodamine [TRITC (tetramethylrhodamine $\beta$-isothiocyanate)]-conjugated goat anti-rabbit for the detection of GFAP, followed by rinsing with TS. Subsequently, the sections were incubated in FITC-conjugated goat anti-mouse IgG (Invitrogen, Paisley, U.K.) for the detection of A$\beta$. All the sections were mounted in an aqueous medium (Vectashield; Vector Laboratories).

## Morphological analysis of the astrocytic cytoskeleton

GFAP-positive astrocytes ($n$=30–35 in single fluorescent labelling experiments) throughout the layer of the LEC were imaged by using confocal microscopy (Leica SP5, Mannheim, Germany) with 0.2 μm $z$-step size. Parallel confocal planes were superimposed and Cell Analyst program (Chvatal et al., 2007) was used for analysis. Five digital filters (average $3 \times 3$, convolution, gauss $5 \times 5$, despeckle, simple objects removal) with a threshold of 50 were used to determine the surface and volume of the GFAP-positive astrocytic cytoskeleton. When analysing astroglial morphology in relation to A$\beta$ plaques, all cells with somata within 50 μm from the plaque border were regarded as plaque associated, and cells with somata located more distantly (>50 μm) as cells not associated with plaques (Olabarria et al., 2010).

## GFAP-IR (glial fibrillary acidic protein-immunoreactive) cell count in the EC

To determine the Nv (numerical density) of GFAP-IR astrocytes in the EC, we counted the number of GFAP-IR astrocytes throughout the layers of the whole LEC, an area

of 435000 μm$^2$ in coronal sections with 40 μm thickness in three or four representative non-consecutive sections. Confocal stack images were used for this purpose. GFAP-IR astrocytes were intensely labelled against dark background, which made them easy to identify with equal chances of being counted. The analysis was performed blindly with regard to mouse genotype.

## Statistical analysis

Data are expressed as means ± S.E.M. The paired or unpaired Student's *t* test was used to examine differences in the Nv, surface, volume and somata volume of GFAP-labelled cells between 3xTg-AD and non-Tg animals, using Graphpad Prism (GraphPad Software, La Jolla, CA, U.S.A.). $P \leqslant 0.05$ was considered statistically significant.

# RESULTS

GFAP-IR cells were widely distributed throughout the EC of both non-Tg and 3xTg-AD mice (Figures 2A–2F), with layers I and VI being the ones showing more GFAP-IR cells and stronger immunoreactivity (Figures 2A and 2B). GFAP-IR showed multiple branched processes extending in different directions from elongated cell bodies (Figures 3D–3G).

## Astrocytic cytoskeletal atrophy in 3xTg-AD mice

From 1 month of age, we observed morphological remodelling of EC astrocytes in 3xTg-AD mice compared with non-Tg animals. The astrocytes in 3xTg-AD animals had reduced primary branches (on average by 26%) originating from the soma and a markedly reduced presence of secondary processes extending from the primary branches (reduced by 30% on average), as well as distal ramifications (reduced by 45%; Figures 3D–3G). These changes indicate a morphological atrophy which was further confirmed by a significant decrease in both the surface and volume of GFAP profiles in the EC of 3xTg-AD animals when compared with non-Tg controls (Figures 3A and 3B). At younger ages (1 month), astrocytes of 3xTg-AD mice showed a significant decrease in GFAP surface when compared with the control. The surface area of GFAP-IR profiles was reduced by 48% (378.45 ± 64.56 μm$^2$ compared with 728.47 ± 96.67 μm$^2$; $P$=0.017; Figure 3A). The volume of GFAP-IR cells in 3xTg-AD was reduced by 54% (115.38 ± 25.82 μm$^3$ compared with 252.94 ± 32.73 μm$^3$; $P$=0.012; Figure 3B). This atrophic glial appearance was sustained through all ages up to 12 months (Figures 3A and 3B). This reduction was significant at 3 and 6 months of age; the surface area was decreased by 44 and 39% (378.56 ± 64.53 μm$^2$ compared with 680.20 ± 53.70 μm$^2$, $P$=0.036; 354.68 ± 67.74 μm$^2$ compared with 581.26 ± 70.13 μm$^2$, $P$=0.025 respectively; Figure 3A). The volume of GFAP-IR cells

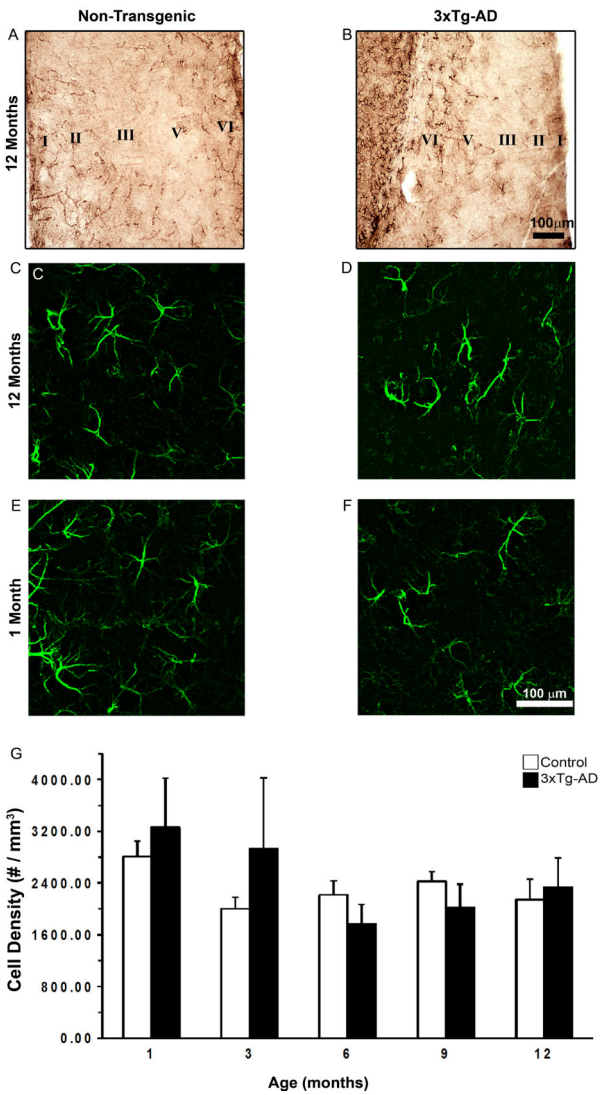


**Figure 2 Comparison of GFAP-IR cell distribution and density in the EC of non-Tg and 3xTg-AD animals**

Bright-field micrographs show the distribution of GFAP-IR astrocytes in the EC of non-Tg and 3xTg-AD animals (**A** and **B** respectively). Confocal imaging shows the organization of GFAP-IR astrocytes in the EC of non-Tg and 3xTg-AD animals at 1 month (**C** and **D** respectively) and 12 months (**E** and **F** respectively) at higher magnification. The histogram shows the Nv (number of cells per mm$^3$) of GFAP-IR cells in the EC of 3xTg-AD and non-Tg controls (**G**). Results are means ± S.E.M.

decreased by 42 and 42% respectively (130.25 ± 25.82 μm$^3$ compared with 224.32 ± 18.80 μm$^3$, $P$=0.0490; 116.15 ± 25.63 μm$^3$ compared with 200.64 ± 31.07 μm$^3$, $P$=0.025 respectively; Figure 3B). However, from 9 months of age onwards the degree of atrophic changes became somewhat less pronounced because of parallel atrophic changes developing in healthy aged controls. At 9 months of age, the surface and volume of astrocytes in 3x-Tg-AD animals were reduced, compared with the control, by 26% (391.04 ± 30.75 μm$^2$ compared with 529.47 ± 48.21 μm$^2$,

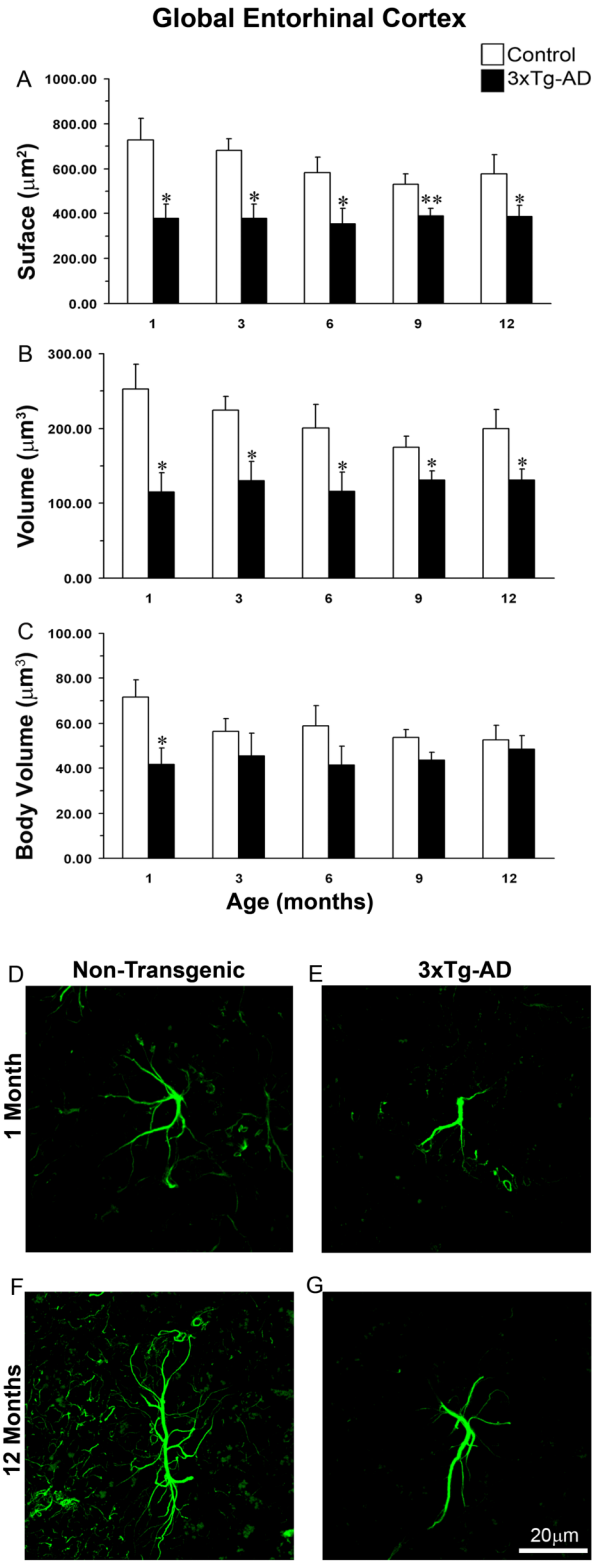


**Figure 3 Comparison of astrocytic GFAP surface and volume in the whole EC of non-Tg and 3xTg-AD animals across ages**

The histograms show a comparison of GFAP (**A**) surface, (**B**) volume and (**C**) body volume in the global EC at the age of 1, 3, 6, 9 and 12 months between 3xTg-AD and non-Tg animals. Results are means ± S.E.M. (*$P \leq 0.05$ compared with the age-matched non-Tg control). Confocal micrographs show astrocytic atrophy in 3xTg-AD at 1 month (**E**) and 12 months (**G**) compared with the control animals (**D** and **F**).

$P=0.008$) and 25% ($130.92 \pm 12.40$ $\mu m^3$ compared with $174.71 \pm 15.41$ $\mu m^3$, $P=0.014$) respectively (Figures 3A and 3B). Likewise, at 12 months of age the decrease in surface and volume was 33% ($387.73 \pm 47.75$ $\mu m^2$ compared with $578.16 \pm 84.46$ $\mu m^2$; $P=0.021$; Figure 3B) and 45% ($130.73 \pm 14.93$ $\mu m^3$ compared with $200.13 \pm 25.18$ $\mu m^3$; $P=0.017$) respectively (Figures 3A and 3B).

This generalized atrophy was also confirmed by a parallel and significant decrease in the somata volume of GFAP-IR astrocytes at a very early age (1 month) ($41.63 \pm 7.43$ $\mu m^3$ compared with $71.69 \pm 7.68$ $\mu m^3$; $P=0.027$; Figure 3C) when compared with control mice. However, at later ages, this decrease in somata volume persisted but became insignificant when compared with non-Tg due to a parallel decrease in non-Tg animals.

## Layer-specific astrocytic atrophy during AD

We found a significant decrease in GFAP-IR cell surface areas in layers II, III and VI of 3xTg-AD animals when compared with controls from 1 month of age by 57% ($323.57 \pm 53.89$ $\mu m^2$ compared with $769.28 \pm 180.91$ $\mu m^2$; $P=0.035$), 45% ($305.36 \pm 70.05$ $\mu m^2$ compared with $564.42 \pm 62.21$ $\mu m^2$; $P=0.031$) and 56% ($416.65 \pm 87.62$ $\mu m^2$ compared with $964.04 \pm 118.84$ $\mu m^2$; $P=0.007$; Figure 4A) respectively. This decrease in the GFAP surface was also paralleled by a reduction in the cell volume in all layers: a reduction in volume of 66% in layer II ($84.78 \pm 17.82$ $\mu m^3$ compared with $251.43 \pm 65.01$ $\mu m^3$; $P=0.028$), 68% in layer III ($59.57 \pm 16.16$ $\mu m^3$ compared with $187.70 \pm 26.64$ $\mu m^3$; $P=0.004$) and 71% in layer VI ($132.08 \pm 44.52$ $\mu m^3$ compared with $360.13 \pm 38.71$ $\mu m^3$; $P=0.0072$; Figure 4B). However, we did not find any significant difference in the other layers, layers I and V.

However, at middle age (6 months), these atrophic changes in surface and volume occurred only in layers II and V. The surface decreased by 38% ($320.53 \pm 71.52$ $\mu m^2$ compared with $520.03 \pm 79.62$ $\mu m^2$; $P=0.021$) and 41% ($386.35 \pm 97.00$ $\mu m^2$ compared with $650.50 \pm 70.60$ $\mu m^2$; $P=0.004$) in layers II and V respectively (Figure 4C); the volume decreased by 45% ($93.74 \pm 24.85$ $\mu m^3$ compared with $169.19 \pm 38.39$ $\mu m^3$; $P=0.023$) and 42% ($130.43 \pm 37.92$ $\mu m^3$ compared with $224.85 \pm 34.16$ $\mu m^3$; $P=0.011$) in layers II and V respectively (Figure 4D). However, no significant decline in either surface or volume was found in layers I, III and VI.

Finally, at later ages (12 months), the decrease in either surface or volume was restricted to layer VI but had a similar significance. 3xTg-AD animals showed a decrease in GFAP surface by 43% ($418.81 \pm 53.84$ $\mu m^2$ compared with $739.91 \pm 56.20$ $\mu m^2$; $P=0.007$) and in volume by 49%

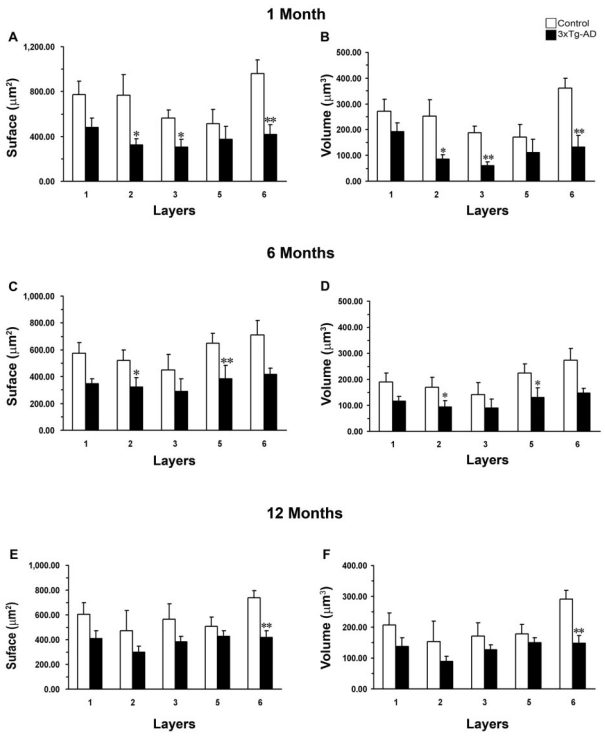


**Figure 4 Comparison of astrocytic GFAP EC surface and volume at different ages**

The histograms show decreased GFAP surface (**A**, **C**, **E**) and volume (**B**, **D**, **F**) within specific layers between 3xTg-AD animals at the ages of 1, 6 and 12 months respectively. Results are means ± S.E.M. (*$P \leq 0.05$; **$P \leq 0.01$ compared with the age-matched non-Tg control).

(149.03 ± 23.85 μm$^3$ compared with 290.03 ± 29.20 μm$^3$; $P = 0.004$; Figures 4E and 4F).

## Astrocytic atrophy in the EC is not associated with loss of GFAP-IR astrocytes

The density of astrocytes in the EC and in different layers of EC of 3xTg-AD mice when compared with non-Tg mice was constant at all ages (Figure 2E). The distribution of GFAP-IR cells throughout the EC was also similar at all ages (Figure 2).

## Rare association of astrocytes with A$\beta$ plaques and absence of hypertrophic reaction

The presence of intraneuronal A$\beta$ accumulation in EC is evident from 9 months of age, although plaques and extracellular aggregates are not present until 12 months of age (Figure 5). However, notwithstanding A$\beta$ accumulation, GFAP-IR astrocytes rarely appear to be associated with A$\beta$-positive neurons, extracellular A$\beta$ aggregates or SPs in the 3xTg-AD animals. All in all, less than 5% of astrocytes were located at a distance <50 μm to the SP. Most importantly, however, we failed to observe any signs of hypertrophy in EC astrocytes in 3xTg-AD animals

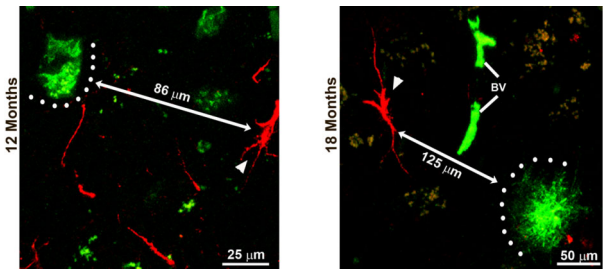


**Figure 5 Distribution and relationship of GFAP immunoreactive astrocytes and β-amyloid presence**

Confocal images of dual labelling of GFAP (red) and A$\beta$ (green) show that GFAP-IR astrocytes are distant from intracellular A$\beta$ deposits (with a distance of 86 μm) at 12 months and distant from the A$\beta$ plaques (with a distance of 125 μm) at 18 months. Arrowheads indicate astrocytes.

at all ages; astroglial cells always demonstrated atrophic morphology.

# DISCUSSION

The EC is regarded as a funnel for cortico-hippocampal information transfer and integration, playing an essential role in cognition and memory (Kerr et al., 2007; Canto et al., 2008; Coutureau and Di Scala, 2009). In the present study, for the first time we present evidence indicating an early (from 1 month of age) atrophy of astrocytes in the EC of 3xTg-AD mice; this atrophy being sustained through more advanced ages (up to 12 months). This atrophic remodelling occurred in the superficial and deep layers at early and middle age (1–6 months), although at later ages (12 months) it remained only in the deeper layers. The morphological atrophy of astroglia is not accompanied by an astrocytic loss at all ages.

The generalized atrophy characterized by a major reduction in astrocytic primary branches and massive reduction in secondary and distal processes in the EC appears in very young 3xTg-AD animals (1 months old), which did not show yet any signs of AD pathology. This atrophic appearance remains in later ages (12 months), distinguished by developed A$\beta$ plaques and NFTs, which are confirmed by the immunoreactivity of A$\beta$ and phosphorylated tau protein (Supplementary Figure S1 at http://www.asnneuro.org/an/003/an003e071add.htm; Oddo et al., 2003b; Rodríguez et al., 2009b). Consistent reduction in the GFAP expression is in agreement with our previous observations of generalized atrophy of astrocytes in the HC, which similarly appear before the neuropathological marks (from 9 months) and are sustained in later ages (up to 18 months; Rodríguez et al., 2009b; Olabarria et al., 2010). Although some post-mortem studies have revealed hypertrophic astrocytes, characteristic of astrogliosis in the EC of AD human patients (Muramori et al., 1998; Porchet et al., 2003, Vanzani et al., 2005), this is only

related to intralaminar astrocytes, since interlaminar astrocytes also showed disrupted processes and dynamic properties (Colombo et al., 2002). Furthermore, microarray analysis also showed a decrease in gene transcription of astrocytic cytoskeleton proteins in AD, implying a down-regulation of the astrocytic cytoskeleton (Simpson et al., 2011). At the same time, the density of GFAP-IR cells remains constant at all ages in both the control and 3xTg-AD. This indicates that neither aging nor AD pathology triggers cell loss. These data again correspond to our previous study and argue against the prominent astroglial proliferative response in the 3xTg-AD brain (Olabarria et al., 2010).

Astrocytic atrophy in the EC occurred very early, at 1 month of age. This is somewhat similar to the general observation that the AD pathology is manifested by A$\beta$ accumulation, which begins in neocortex and rhinal cortices, including the EC, subsequently progressing to the HC and eventually appearing in all subcortical areas (Braak and Braak, 1997; Thal et al., 2000). The formation of neurofibrillary tangles initiates in the transentorhinal as well as entorhinal cortices, advancing to the HC through the perforant path and neighbouring cortical regions (Braak et al., 1999). The spatiotemporal occurrence of astroglial atrophy is therefore consistent with pathological hallmarks of AD, indicating that the EC is the region first affected by AD pathology. The evident changes in entorhinal astrocytes appear within layers II, III and VI at early age (1 month); layers II and V are affected at middle age (6 months), while they are restricted in layer VI at later ages (12 months). Nevertheless, it should be noted that there is no recovery of atrophic astrocytes in transgenic mice in the superficial layers at later ages but a decrease in GFAP in non-Tg controls, implying an aging effect on control animals (Figure 3).

Astroglia sustain multiple functions, including balance of neurotransmitters, release of trophic factors, metabolic support and extracellular ion buffering, all of which maintain brain physiology and support neuronal connectivity (Danbolt, 2001; Nedergaard et al., 2003; Wang and Bordey, 2008; Verkhratsky et al., 2010, 2011). In addition, astrocytes are able to sense synaptic activity, regulate synaptic plasticity and synchronize neuronal networks, thus being involved in conscience and cognitive processes (Araque et al., 1999; Fellin et al., 2004; Henneberger et al., 2010; Lalo et al., 2006, 2011). Finally, by virtue of astrogliosis, astrocytes form the innate brain defence system, localizing the lesions and assisting in pathological remodelling of the affected circuitry (Sofroniew, 2009). Early astroglial atrophy observed in EC may result in reduced astroglial coverage of synapses and thus may appear to be a key factor in altered synaptic connectivity (Rodríguez et al., 2009b; Verkhratsky et al., 2010). In consequence, the synaptic condition and/or activity may be affected, causing synaptic remodelling, altered synaptic connections and network activity. It is likely that this early astrocytic alteration leads to compromised EC output to other areas, especially the HC that receives innervation from both the superficial and deep layers of the EC (Figure 1). In fact, there is no significant neuronal loss in memory-associated areas, such as the EC and HC, in the 3xTg-AD animal model (Oddo et al., 2003a, 2003b; Rohn et al., 2008; Bittner et al., 2010). Nonetheless, loss of synapses and/or dendritic spines as well as compromised long-term potentiation have been detected in several brain regions, suggesting impaired synaptic connectivity and functions in this animal model (Oddo et al., 2003a; Bertoni-Freddari et al., 2008; Bittner et al., 2010; Noristani et al., 2011). Therefore the astrocytic atrophy in the EC may underlie synaptic pathology being the basis of cognitive and memory impairment at the early stages of the AD.

In contrast with the HC (Olabarria et al., 2010), arrival of A$\beta$ depositions and SPs in the EC does not trigger astrolgiotic reaction at least from the morphological criteria. We failed to observe a close association of astrocytes with SPs; nor did we find any signs of astroglial hypertrophy. This peculiar indifference of EC astrocytes to the AD-specific lesion may underlie the particular vulnerability of the EC to the AD-like pathology and provide an explanation of why EC is the first brain region to be affected in the course of AD. Obviously, further studies are required to extend the findings from the AD animal model to human pathology.

**FUNDING**

This work was supported by an Alzheimer's Research Trust's Programme Grant [grant number ART/PG2004A/1 (to J.J.R. and A.V.)]; the Grant Agency of the Czech Republic [grant numbers GACR 309/09/1696 and GACR 304/11/0184 (to J.J.R.) and GACR 305/08/1381 and GACR 305/08/1384 (to A.V.)]; the Spanish Government, Plan Nacional de I+D+I 2008–2011 and ISCIII-Subdirección General de Evaluación y Fomento de la investigación [grant number PI10/02738 (to J.J.R. and A.V.)]; and the Government of the Basque Country grants [grant numbers AE-2010-1-28 and AEGV10/16 (to J.J.R.)].

## REFERENCES

Araque A, Parpura V, Sanzgiri RP, Haydon PG (1999) Tripartite synapses: glia, the unacknowledged partner. Trends Neurosci 22:208–215.

Bertoni-Freddari C, Sensi SL, Giogetti B, Balietti M, Di Stefano G, Canzoniero LM, Casoli T, Fattoretti P (2008) Decreased presence of perforated synapses in a triple-transgenic mouse model of Alzheimer's disease. Rejuvenation Res 11:309–313.

Billings LM, Oddo S, Green KN, McGaugh JL, La Ferla FM (2005) Intraneuronal Abeta causes the onset of early Alzheimer's disease-related cognitive deficits in transgenic mice. Neuron 45:675–688.

Bittner T, Fuhrmann M, Burgold S, Ochs SM, Hoffmann N, Mitteregger G, Kretzschmar H, LaFerla FM, Herms J (2010) Multiple events lead to dendritic spine loss in triple transgenic Alzheimer's disease mice. PLoS One 5:e15477.

Braak H, Braak E (1991) Neuropathological staging of Alzheimer-related changes. Acta Neuropathol 82:239–259.

Braak H, Braak E (1997) Frequency of stages of Alzheimer-related lesions in different age categories. Neurobiol Aging 18:351–357.

Braak E, Griffing K, Arai K, Bohl J, Bratzke H, Braak H (1999) Neuropathology of Alzheimer's disease: what is new since A. Alzheimer? Eur Arch Psychiatry Clin Neurosci 249 (Suppl. 3):14–22.

Calhoun ME, Wiederhold KH, Abramowski D, Phinney AL, Probst A, Sturchler-Pierrat C, Staufenbiel M, Sommer B, Jucker M (1998) Neuron loss in APP transgenic mice. Nature 395:755–756.

Canto CB, Wouterlood FG, Witter MP (2008) What does the anatomical organization of the entorhinal cortex tell us? Neural Plast 2008: 381243.

Chvatal A, Anderova M, Hock M, Prajerova I, Neprasova H, Chvatal V, Kirchhoff F, Sykova E (2007) Three-dimensional confocal morphometry reveals structural changes in astrocyte morphology *in situ*. J Neurosci Res 85:260–271.

Colombo JA, Quinn B, Puissant V (2002) Disruption of astroglial interlaminar processes in Alzheimer's disease. Brain Res Bull 58:235–242.

Coutureau E, Di Scala G (2009) Entorhinal cortex and cognition. Prog Neuropsychopharmacol Biol Psychiatry 33:753–761.

Craig S, Commins S (2005) Interaction between paired-pulse facilitation and long-term potentiation in the projection from hippocampal area CA1 to the entorhinal cortex. Neurosci Res 53:140–146.

Cunningham MO, Hunt J, Middleton S, LeBeau FE, Gillies MJ, Davies CH, Maycox PR, Whittington MA, Racca C (2006) Region-specific reduction in entorhinal gamma oscillations and parvalbumin-immunoreactive neurons in animal models of psychiatric illness. J Neurosci 26:2767–2776.

Danbolt NC (2001) Glutamate uptake. Prog Neurobiol 65:1–105.

de Toledo-Morrell L, Goncharova I, Dickerson B, Wilson RS, Bennett DA (2000) From healthy aging to early Alzheimer's disease: *in vivo* detection of entorhinal cortex atrophy. Ann N Y Acad Sci 911:240–253.

Du AT, Schuff N, Amend D, Laakso MP, Hsu YY, Jagust WJ, Yaffe K, Kramer JH, Reed B, Norman D, Chui HC, Weiner MW (2001) Magnetic resonance imaging of the entorhinal cortex and hippocampus in mild cognitive impairment and Alzheimer's disease. J Neurol Neurosurg Psychiatry 71:441–447.

Fellin T, Pascual O, Gobbo S, Pozzan T, Haydon PG, Carmignoto G (2004) Neuronal synchrony mediated by astrocytic glutamate through activation of extrasynaptic NMDA receptors. Neuron 43:729–743.

Fransen E (2005) Functional role of entorhinal cortex in working memory processing. Neural Netw 18:1141–1149.

Fyhn M, Molden S, Witter MP, Moser EI, Moser MB (2004) Spatial representation in the entorhinal cortex. Science 305:1258–1264.

Goedert M, Jakes R, Vanmechelen E (1995) Monoclonal antibody AT8 recognises atu protein phosphorylation at both serine 202 and threonine 205. Neurosci Lett 189:167–170.

Gomez-Isla T, Price JL, McKeel Jr DW, Morris JC, Growdon JH, Hyman BT (1996) Profound loss of layer II entorhinal cortex neurons occurs in very mild Alzheimer's disease. J Neurosci 16:4491–4500.

Halliday GM, Cullen KM, Kril JJ, Harding AJ, Harasty J (1996) Glial fibrillary acidic protein (GFAP) immunohistochemistry in human cortex: a quantitative study using difference antisera. Neurosci Lett 209:29–32.

Halliday GM, Double KL, Macdonald V, Kril JJ (2003) Identifying severely atrophic cortical subregions in Alzheimer's disease. Neurobiol Aging 24:797–806.

Harciarek M, Jodzio K (2005) Neuropsychological differences between frontotemporal dementia and Alzheimer's disease: a review. Neuropsychol Rev 15:131–145.

Heneka MT, Rodríguez, JJ, Verkhratsky A (2010) Neuroglia in neurodegeneration. Brain Res Rev 63:189–211.

Henneberger C, Papouin T, Oliet SH, Rusakov DA (2010) Long-term potentiation depends on release of D-serine from astrocytes. Nature 463:232–236.

Kerr KM, Agster KL, Furtak SC, Burwell RD (2007) Functional neuroanatomy of the parahippocampal region: the lateral and medial entorhinal areas. Hippocampus 17:697–708.

Kordower JH, Chu Y, Stebbins GT, DeKosky ST, Cochran EJ, Bennett D, Mufson EJ (2001) Loss and atrophy of layer II entorhinal cortex neurons in elderly people with mild cognitive impairment. Ann Neurol 49:202–213.

Kril JJ, Patel S, Harding AJ, Halliday GM (2002) Neuron loss from the hippocampus of Alzheimer's disease exceeds extracellular neurofibrillary tangle formation. Acta Neuropathol 103:370–376.

Lalo U, Pankratov Y, Kirchhoff F, North RA, Verkhratsky A (2006) NMDA receptors mediate neuron-to-glia signaling in mouse cortical astrocytes. J Neurosci 26:2673–2683.

Lalo U, Pankratov Y, Parpura V, Verkhratsky A (2011) Ionotropic receptors in neuronal-astroglial signalling: what is the role of 'excitable' molecules in non-excitable cells. Biochim Biophys Acta 1813:992–1002.

McGaughy J, Koene RA, Eichenbaum H, Hasselmo ME (2005) Cholinergic deafferentation of the entorhinal cortex in rats impairs encoding of novel but not familiar stimuli in a delayed nonmatch-to-sample task. J Neurosci 25:10273–10281.

Moser EI, Kropff E, Moser MB (2008) Place cells, grid cells, and the brain's spatial representation system. Annu Rev Neurosci 31:69–89.

Muramori F, Kobayashi K, Nakamura I (1998) A quantitative study of neurofibrillary tangles, senile plaques and astrocytes in the hippocampal subdivisions and entorhinal cortex in Alzheimer's disease, normal controls and non-Alzheimer neuropsychiatric diseases. Psychiatry Clin Neurosci 52:593–599.

Naber PA, Lopes da Silva FH, Witter MP (2001) Reciprocal connections between the entorhinal cortex and hippocampal fields CA1 and the subiculum are in register with the projections from CA1 to the subiculum. Hippocampus 11:99–104.

Nagele RG, Wegiel J, Venkataraman V, Imaki H, Wang KC (2004) Contribution of glial cells to the development of amyloid plaques in Alzheimer's disease. Neurobiol Aging 25:663–674.

Nedergaard M, Ransom B, Goldman SA (2003) New roles for astrocytes: redefining the functional architecture of the brain. Trends Neurosci 26:523–530.

Noristani HN, Olabarria M, Verkhratsky A, Rodríguez JJ (2010) Serotonin fibre sprouting and increase in serotonin transporter immunoreactivity in the CA1 area of hippocampus in a triple transgenic mouse model of Alzheimer's disease. Eur J Neurosci 32:71–79.

Noristani HN, Meadows RS, Olabarria M, Verkhratsky A, Rodríguez JJ (2011) Increased hippocampal CA1 density of serotonergic terminals in a triple transgenic mouse model of Alzheimer's disease: an ultrastructural study. Cell Death Dis 2:e210.

Oddo S, Caccamo A, Kitazawa M, Tseng BP, LaFerla FM (2003a) Amyloid deposition precedes tangle formation in a triple transgenic model of Alzheimer's disease. Neurobiol Aging 24:1063–1070.

Oddo S, Caccamo A, Shepherd JD, Murphy MP, Golde TE, Kayed R, Metherate R, Mattson MP, Akbari Y, LaFerla FM (2003b) Triple-transgenic model of Alzheimer's disease with plaques and tangles: intracellular Abeta and synaptic dysfunction. Neuron 39:409–421.

Olabarria M, Noristani HN, Verkhratsky A, Rodríguez JJ (2010) Concomitant astroglial atrophy and astrogliosis in a triple transgenic animal model of Alzheimer's disease. Glia 58:831–838.

Paxinos G, Franklin K (2004) The Mouse Brain in Stereotaxic Coordinates, compact 2nd edn, Academic Press, San Diego, CA.

Porchet R, Probst A, Bouras C, Draberova E, Draber P, Riederer BM (2003) Analysis of glial acidic fibrillary protein in the human entorhinal cortex during aging and in Alzheimer's disease. Proteomics 3:1476–1485.

Ranganath C, Johnson MK, D'Esposito M (2003) Prefrontal activity associated with working memory and episodic long-term memory. Neuropsychologia 41:378–389.

Remondes M, Schuman EM (2004) Role for a cortical input to hippocampal area CA1 in the consolidation of a long-term memory. Nature 431:699–703.

Ribe EM, Perez M, Puig B, Gich I, Lim F, Cuadrado M, Sesma T, Catena S, Sanchez B, Nieto M, Gomez-Ramos P, Moran MA, Cabodevilla F, Samaranch L, Ortiz L, Perez A, Ferrer I, Avila J, Gomez-Isla T (2005) Accelerated amyloid deposition, neurofibrillary degeneration and neuronal loss in double mutant APP/tau transgenic mice. Neurobiol Dis 20:814–822.

Rodrigue KM, Raz N (2004) Shrinkage of the entorhinal cortex over five years predicts memory performance in healthy adults. J Neurosci 24:956–963.

Rodríguez JJ, Jones VC, Tabuchi M, Allan SM, Knight EM, LaFerla FM, Oddo S, Verkhratsky A (2008) Impaired adult neurogenesis in the dentate gyrus of a triple transgenic mouse model of Alzheimer's disease. PLoS One 3:e2935.

Rodríguez JJ, Jones VC, Verkhratsky A (2009a) Impaired cell proliferation in the subventricular zone in an Alzheimer's disease model. Neuroreport 20:907–912.

Rodríguez JJ, Olabarria M, Chvatal A, Verkhratsky A (2009b) Astroglia in dementia and Alzheimer's disease. Cell Death Differ 16:378–385.

Rodríguez JJ, Verkhratsky A (2011) Neuroglial roots of neurodegenerative diseases? Mol Neurobiol 43:87–96.

Rohn TT, Vyas V, Hernandez-Estrada T, Nichol KE, Christie LA, Head E (2008) Lack of pathology in a triple transgenic mouse model of Alzheimer's disease after overexpression of the anti-apoptotic protein Bcl-2. J Neurosci 28:3051–3059.

Schneider A, Mandelkow E (2008) Tau-based treatment strategies in neurodegenerative diseases. Neurotherapeutics 5:443–457.

Schwarcz R, Witter MP (2002) Memory impairment in temporal lobe epilepsy: the role of entorhinal lesions. Epilepsy Res 50:161–177.

Simpson JE, Ince PG, Shaw PJ, Heath PR, Raman R, Garwood CJ, Gelsthorpe C, Baxter L, Forster G, Matthews FE, Brayne C, Wharton SB (2011) Microarray analysis of the astrocyte transcriptome in the aging brain: relationship to Alzheimer's pathology and APOE genotype. Neurobiol Aging 32:1795–1807.

Sofroniew MV (2009) Molecular dissection of reactive astrogliosis and glial scar formation. Trends Neurosci 32:638–647.

Solodkin A, Veldhuizen SD, Van Hoesen GW (1996) Contingent vulnerability of entorhinal parvalbumin-containing neurons in Alzheimer's disease. J Neurosci 16:3311–3321.
Suzuki WA, Amaral DG (1994) Topographic organization of the reciprocal connections between the monkey entorhinal cortex and the perirhinal and parahippocampal cortices. J Neurosci 14:1856–1877.
Tamamaki N, Nojyo Y (1993) Projection of the entorhinal layer II neurons in the rat as revealed by intracellular pressure-injection of neurobiotin. Hippocampus 3:471–480.
Thal DR, Schultz C, Dehghani F, Yamaguchi H, Braak H, Braak E (2000) Amyloid beta-protein (Abeta)-containing astrocytes are located preferentially near N-terminal-truncated Abeta deposits in the human entorhinal cortex. Acta Neuropathol 100:608–617.
Vanzani MC, Iacono RF, Caccuri RL, Berria MI (2005) Immunochemical and morphometric features of astrocyte reactivity vs. plaque location in Alzheimer's disease. Medicina (B Aires) 65:213–218.
Verkhratsky A, Olabarria M, Noristani HN, Yeh CY, Rodríguez JJ (2010) Astrocytes in Alzheimer's disease. Neurotherapeutics 7:399–412.
Verkhratsky A, Parpura V, Rodríguez JJ (2011) Where the thoughts dwell: the physiology of neuronal-glial 'diffuse neural net'. Brain Res Rev 66:133–151.
Wang DD, Bordey A (2008) The astrocyte odyssey. Prog Neurobiol 86:342–367.
Whitwell JL, Josephs KA, Murray ME, Kantarci K, Przybelski SA, Weigand SD, Vemuri P, Senjem ML, Parisi JE, Knopman DS, Boeve BF, Petersen RC, Dickson DW, Jack Jr CR (2008) MRI correlates of neurofibrillary tangle pathology at autopsy: a voxel-based morphometry study. Neurology 71:743–749.
Witter MP, Van Hoesen GW, Amaral DG (1989) Topographical organization of the entorhinal projection to the dentate gyrus of the monkey. J Neurosci 9:216–228.
Witter MP and Amaral DG (2004) Hippocampal formation. In: The Rat Nervous System, 3 Edition (Paxinos G, ed), pp. 635–704, San Diego, CA: Academic Press.

**Received 18 August 2011/10 October 2011; accepted 14 October 2011**
**Published as Immediate Publication 21 November 2011, doi 10.1042/AN20110025**